Contact angle hysteresis on nonwetting microstructured surfaces: Effect of randomly distributed pillars or holes

Pavel Iliev ,* Nina Pesheva ,† and Stanimir Iliev‡
Institute of Mechanics, Bulgarian Academy of Sciences, Acad. G. Bonchev St. 4, 1113 Sofia, Bulgaria

(Received 26 January 2024; accepted 12 July 2024; published 6 August 2024)

We present a numerical study of the advancing and receding apparent contact angles for a liquid meniscus in contact with an ultrahydrophobic surface with randomly distributed microsized pillars or holes in the Cassie's wetting regime. We study the Wilhelmy plate system in the framework of the full capillary model to obtain these angles using the heterogeneous surface approximation model for a broad interval of values of pillar or hole concentration and for both square and circular shapes of the pillars or holes cross-section. Three types of random placing of defects on the plate are investigated, i.e., two with restrictions: (1) with maximum and (2) with minimum distance between the defects (in these cases the defects are isolated), and (3) without restrictions (the defects can overlap). The results show that the type of defect distribution and also the type of the defects shape (circular or square) does not affect the magnitude of the two angles. The results of the numerical simulations showed that the retention force for a plate with randomly located defects is not greater, and for larger concentrations of pillars or holes, it is smaller than that for periodically spaced ones. Comparisons with experimental results for the receding contact angle on surfaces with pillars and with the advancing contact angle on surfaces with periodically arranged holes is carried out.

DOI: 10.1103/PhysRevE.110.024801

I. INTRODUCTION

At the forefront of wetting phenomena research lies the investigation into the characteristics of a liquid interacting with microstructured surfaces, comprising arrays of pillars or holes [1]. These type of surfaces, having physical defects, are termed rough. Let us shortly recall that on ideal (flat and chemically homogeneous) surfaces the contact of the liquid with such surface in partial wetting regime is characterized by a unique equilibrium contact angle (CA) θ_{eq}, given by Young's equation (in the framework of the full capillary theory) [2]. However, most real surfaces are by far not ideal, they have different defects physical and/or chemical (in the later case, i.e., only chemical defects, the surface is called chemically heterogeneous). On such nonideal surfaces the equilibrium CA is not any longer unique. At macroscopic level one observes a whole interval $[\theta^r, \theta^a]$ of macroscopic equilibrium CAs and this phenomenon is called contact angle hysteresis (CAH). The lower limit θ^r of the CAH interval is termed receding contact angle (RCA) and the upper limit θ^a is called advancing contact angle (ACA) [3]. When studying the Wilhelmy plate system (a vertical solid plate, immersed in a tank of liquid) the RCA is measured when the plate withdraws from the liquid and the ACA is determined when the plate immerses in the liquid. For the other often studied system, that of a liquid drop on a solid surface, the RCA and the ACA, are uniquely determined at the moment when the drop on inclined surface loses stability and starts to slide down.

Recently, the research interest on wetting phenomena was drawn to a specific realizations of rough solid surfaces—surfaces on which pillars of micrometer size are distributed. On such surfaces (known as microstructured surfaces), when in contact with a liquid, gas bubbles (or air pockets) are formed on some parts of the liquid and solid contact. A similar effect is observed when instead of pillars there are arrays of holes on the surface. This type of regime of liquid and solid contact is termed Cassie's wetting regime and it leads to a sharp decrease of the CAH. This in turn is the reason for heightened interest in studying such type of surfaces. A minimal CAH proves highly beneficial for numerous technological processes, motivating an interest in exploring and understanding better this problem. In numerous experimental works, artificially formed surfaces with physical defects of the same shape and size (pillars or holes) are used. The cross-sections of these defects are most commonly square or circular, but there are also rhomboid, star-shaped, or other shapes [4–7]. When investigating how the concentration, size, shape, and arrangement of defects affect the CAH, surfaces with periodically arranged defects are most commonly used with a square, rectangular, as well as hexagonal distribution.

A. CAH on microstructured surfaces

For these types of surfaces, it is established that there is a certain asymmetry in the behavior of the CAH for the two types of microstructured surfaces (i.e., covered with pillars and, respectively, with holes). It has been established [8] that the ACA for pillars $\theta^{a(p)}$ and the RCA for holes $\theta^{r(h)}$ are constants that do not depend on the type and concentration of defects, while the RCA for pillars $\theta^{r(p)}$ and the ACA for

*Contact author: piliev@imbm.bas.bg
†Contact author: nina@imbm.bas.bg
‡Contact author: stani@imbm.bas.bg

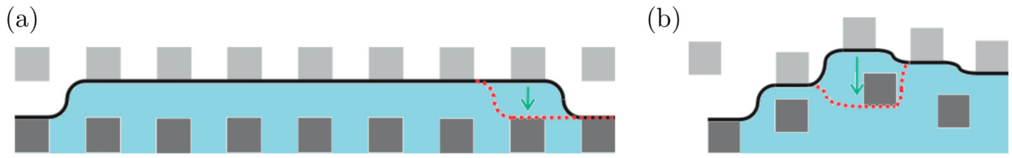

FIG. 1. Schematic drawing of a CL kink depinning mechanism in the CL receding regime: (a) at periodic defects (replica of Fig. 9(b) in Ref. [11]), and (b) at random defects.

holes $\theta^{a(h)}$ depend on the defect concentration. Due to that property, the problem of finding the CAH on such surfaces is reduced to the determination of the $\theta^{r(p)}$, respectively, $\theta^{a(h)}$, depending on the type of surface roughness (surface with pillars or, respectively, with holes). These angles ($\theta^{r(p)}$ and $\theta^{a(h)}$) depend on the parameters, characterizing the surface roughness, i.e., the distribution (including the type of arrangement of defects and concentration), the size of the physical defects, and the equilibrium CA, which the liquid forms with the solid phase. The experimental studies show, that even in the case of surfaces with pillars or holes whose size is just few micrometers, the solid phase cannot be treated as ideal, i.e., the solid phase is rough and/or heterogeneous [9–11], though at finer scale. The simplest possible way to account for this fact is to consider the existence of an intrinsic CAH [θ_s^r, θ_s^a] (s—solid) of the solid phase and, respectively, to consider how it affects the values of the $\theta^{r(p)}$ and $\theta^{a(h)}$. In the present work, we will adopt this simplified approach as in other research on CAH, see, e.g., Refs. [10,12–15]. Thus, following this approach, simple theoretical reasoning shows that $\theta^{a(p)} = 180^\circ$ and $\theta^{r(h)} = \theta_s^r$. This behavior contrasts with that of the $\theta^{r(p)}$ and the $\theta^{a(h)}$. The prevailing understanding is that the $\theta^{r(p)}$ and $\theta^{a(h)}$ are unique functions of the *defect surface fraction* p [8,16] (i.e., the ratio between the total contact area on the tops of the pillars or holes and the total projected solid area) and of the *defect line fraction* ϕ [17,18] (the ratio between the length of the part of the equilibrium contact line (CL) that passes through pillars or holes and the length of the entire CL; usually, ϕ is estimated as the ratio of the pillar or hole size to the cell size along the line connecting the centers of the pillars or holes). When studying the effect of the defect line fraction, then the CL refers to the three-phase CL of the *reduced problem* (or else the heterogeneous surface approximation model), in which the physical defects, such as pillars or holes are replaced with chemical defects on a smooth surface, where the liquid forms a continuous CL with the heterogeneous surface [19].

B. Role of depinning mechanism on CAH

In the heterogeneous surface approximation of the initial problem (liquid contact with a rough surface) on the segments of the CL that are not in contact with the solid phase, the contact angle $\theta_v = 180^\circ$ (v—vapor) is assumed. Numerical simulations show that studying the reduced problem (instead of the original) does not affect the magnitude of the CAH [20]. Under the assumption that the three-phase contact line is located on one row of pillars or holes, it is theoretically justified [18] and numerically confirmed [21] that the $\theta^{r(p)}$ and $\theta^{a(h)}$ are unique functions of the defect line fraction ϕ, where the $\theta^{r(p)}$ and $\theta^{a(h)}$ are equal to the modified Cassie angle, in which the area fraction p is replaced by the line fraction ϕ, i.e., one has

$$\cos\theta^{r(p)} = \phi\cos\theta_s^r + (1-\phi)\cos\theta_v, \tag{1}$$

$$\cos\theta^{a(h)} = (1-\phi)\cos\theta_s^a + \phi\cos\theta_v. \tag{2}$$

The provided formulas in Eqs. (1) and (2) have a limited validity since the assumptions made for their derivation are not always fulfilled. In reality, the CL is not always located on a single row of pillars or holes. For a liquid droplet on a surface with pillars, Dorrer and Rühe [11] have indicated that it is improbable that the CL may dewet over its entire length at once (*block depinning regime*). According to them, receding motion would be split into a series of jumping events (*kink depinning regime*), resulting in a step function running along the contact line, as it is illustrated in Fig. 1(a) (which is a replica of Fig. 9(b) in Ref. [11]). Figure 1(a) shows a schematic illustration of a CL kink depinning mechanism in the receding regime, appearing on a rough surface with pillars arranged in a square lattice, when looking from above (i.e., from a direction, perpendicular to the solid plate). The initial CL is denoted by a thick solid line, and the gas and the liquid phases are above and below the CL, respectively. The direction of the CL depinning is shown by an arrow. The dashed line denotes the part of the CL which has moved in the depinning process. Each of these movements of the CL line occurs at the places between two adjacent rows of pillars, i.e., in the receding regime, the CL loses stability at the areas, where it switches between two adjacent rows of pillars.

This assumption has been experimentally confirmed [16,22] and supported also by numerical simulations [24]. The obtained experimental results for the $\theta^{r(p)}$ indicate that it is significantly larger than the predicted by Eq. (1), i.e., considering the appearing of a kink depinning leads to a decrease of the CAH. The experimental results for the $\theta^{r(p)}$ are consistent with the numerical simulations for the $\theta^{r(p)}$ in Refs. [22] and [20], using different software implementation, i.e., SURFACE EVOLVER [23] and the Local variations method, respectively. Studies on the $\theta^{r(p)}$ with different designs of the periodic arrangement of pillars, i.e., square, rectangular, and hexagonal lattices, and at various concentrations of pillars, have shown that the $\theta^{r(p)}$ depends uniquely on the defect surface fraction but not on the defect line fraction. For periodically arranged pillars, the mentioned scenario occurs during the receding motion of the CL but not during the advancement of the CL [24].

C. How do the values of the CAH compare on surfaces with periodically and randomly distributed pillars or holes?

The existence of two types of CL depinning for periodically arranged defects leads to asymmetric wetting hysteresis. However, whether the periodic arrangement is indeed one of the reasons for a small CAH is an interesting question. The consistency of the $\theta^{r(p)}$ values for different arrangements of periodic defects shows that the depinning moment depends weakly on the mutual arrangement of pillars located in the region where the CL passes from one row of pillars to another. A similar situation occurs when the pillars are randomly placed and not arranged in rows of periodic defects, as illustrated in Fig. 1(b). In this case, every movement of the CL is of the kink type, occurring both during the receding and the advancement of the CL.

In view of the above discussion the following question arises: How do the values of the CAH compare on surfaces with periodically and randomly distributed pillars or holes, given equal all remaining parameters (defect shape, concentration, θ_s^r, θ_s^a)? The answer to this still largely unexplored question is the main subject of the present study. Its relevance is determined by the fact that manifestations of the lotus effect in nature occur on surfaces with randomly arranged localized pillars (this is how they are arranged on lotus leaves [25,26]; examples of randomly arranged physical defects can be found in Refs. [6,27–31]). For this purpose, numerical calculations of the ACA and the RCA will be obtained for surfaces with pillars or holes and a comparison will be made with the case where the pillars or holes form a doubly periodic structure where kink CL depinning occurs. For simplicity, we will consider the reduced problem where the solid surface is considered flat but covered with chemical defects.

II. PROBLEM FORMULATION

A. Wilhelmy plate with heterogeneous surface

The Wilhelmy balance geometry is used in this study, conventionally employed for CA determination. It is assumed that the square plate Ξ (dipped in a tank of liquid) with a side length a, is vertical. In Cartesian coordinates $(x,\ y,\ z)$, where the z-axis is oriented opposite to the gravitation force the vertical plate Ξ is defined as $\Xi \equiv \{x = 0,\ 0 \leqslant y \leqslant a, -a/2 \leqslant z \leqslant a/2\}$. We consider that the square plate has a heterogeneous but smooth solid surface consisting of a homogeneous base (on which the liquid forms an equilibrium CA in the range $[\theta_B^r, \theta_B^a]$ (B—base), on which defects are placed. These defects are characterized by the equilibrium CA which the liquid forms on them, taking values in the range $[\theta_D^r, \theta_D^a]$ (D—defect). Heterogeneous surfaces, for which one has $\theta_B^r > \theta_D^a$, will be referred as “pillar”-type surfaces and when $\theta_D^r > \theta_B^a$ as “hole”-type surfaces. For the purpose of comparing the obtained results conveniently with the available experimental data, we assume that the liquid in consideration is water as in Ref. [16]. We investigate the effect of two different defect shapes: circular defects with a radius $r = 5\,\mu$m (similarly to Ref. [16]) and square defects with a side $b = r\sqrt{\pi}$ (the sizes of the two types of defects are chosen in such way so that the areas of the cross-sections of the two types of defects are equal), with the sides of the square defects parallel to the edges of the plate.

B. Types of defect distributions

We will consider three methods for generation of defects on the solid surface. To gradually differentiate from the case of periodic defects, where defects are isolated, (i.e., the distance between the defect centers is bigger than the diameter $2r = 10\,\mu$m in the case of circular defects and bigger than the square diagonal $r\sqrt{2\pi} \approx 12.53\,\mu$m in the case of square defects) and spaced at a large distance, we will create the following distributions:

Distribution Type I, where $N = a^2/(\pi r^2)$ defect centers are placed sequentially on the square domain using a random number generator, ensuring that the minimum distance between the defects is as large as possible. This is achieved in the following way. We first define a new variable λ, initialized with $\lambda = 2r$ for defects of circular shape and $\lambda = b$ for defects of square shape. Next, we generate successively N defect centers with the condition that the distance between each pair of centers is $\geqslant \lambda$. This procedure is repeated several times with increasing λ, until it is no longer possible to place all N centers within the square with size a with the prescribed constraints. The largest value of λ for which the procedure was successful is used for the realization of the defect structure approximating the randomly distributed defects. The obtained value of λ as a result of this procedure is a function of the defect surface fraction p, and it decreases with p. For example, for defect size $r = 5\,\mu$m (or $b = r\sqrt{\pi}$), one has $\lambda = 33.6\,\mu$m at $p = 0.05$, $\lambda = 19.1\,\mu$m at $p = 0.15$, $\lambda = 13.4\,\mu$m at $p = 0.30$ (for a circular and square shaped defects), and $\lambda = 11\,\mu$m at $p = 0.45$ (only in the case of circular defects). A possible realization of this defect distribution is shown in Figs. 7(a) and 8(a) in the Appendix in the case of circular defects at concentration $p = 0.1$ and $p = 0.4$, correspondingly.

Distribution Type II is similar to type I, where the N defects are placed sequentially, but the only condition in this case is that the centers are spaced at a fixed minimum distance $\lambda = 11\,\mu$m for circular defects and $\lambda = 12.6\,\mu$m for square defects. These distances ensure that the defects are isolated. An example of this distribution is shown in Figs. 7(b) and 8(b) in the Appendix, at concentration $p = 0.1$ and $p = 0.4$, correspondingly, where the defects are also of circular shape.

These two types (I and II) of placing randomly isolated identical defects allow for the investigation of concentrations up to $p = 0.45$ for circular defects, and $p = 0.34$ for square defects. In the case of circular defects at $p = 0.45$, one gets that in distributions type I and type II the distance parameter λ between defects is one and the same, i.e., one gets $\lambda = 11\,\mu$m. The same is observed also for square defects, however at $p = 0.34$, one gets that in both types (I and II) of defect distributions. The difference in the maximal considered concentrations for circular defects and square defects comes from their different shapes and the imposed requirement that the defects are isolated. For circular defects, the requirement that the defects are isolated means that the defect centers should be at a distance, bigger than their diameter $2r = 10\,\mu$m. In the case of square defects (whose size is $b = 8.86\,\mu$m) the requirement that the defects are isolated means that the defect centers should be at a distance >12.54 μm (which is the size of the square diagonal). This requirement results in maximal considered concentration of $p = 0.34$ for square defects, while for circular defects it is $p = 0.45$.

Distribution Type III involves generating randomly arranged defects where overlapping between the defects is allowed. The total number of defects is increased compared to the previous two types, while maintaining the same concentration as in the above two cases. An illustration of this distribution is shown in Figs. 7(c) and 8(c) in the Appendix at concentration $p = 0.1$ and $p = 0.4$, respectively, for circular defects.

The studies for circular shaped defects show that the correlation between defects at distances bigger than the defect diameter $2r$ is small for all types I–III (see the Appendix for more details).

To compare the CAH on surfaces having randomly distributed defects (distributions types I–III) with periodically structured surfaces, we calculate the CAH also on surfaces with the following distribution:

Distribution Type IV has periodically distributed defects with centers arranged in a square lattice.

C. ACA and RCA determination

The ACA and the RCA are calculated based on the equilibrium states of the liquid meniscus in contact with a heterogeneous square plate. The relation between the averaged macroscopic CA θ and the averaged contact line (CL) height $\langle h(y)\rangle_y$ of the liquid meniscus is used [21,32,33] for the determination of the CA:

$$\theta = \arcsin\left(1 - \langle h\rangle^2 / 2l_c^2\right), \tag{3}$$

where $l_c = \sqrt{\gamma/\rho g}$ is the capillary length, γ is liquid-gas surface tension, ρ is the difference of the densities of the liquid in the tank and the ambient gas, and g is the gravity acceleration (in a study of capillary rise the effect of gravitation cannot be ignored). This definition of the angle θ is deduced from the CL height h via a well known relation between the contact angle θ and the CL height h on an ideally homogeneous flat wall [34],

$$h = l_c\sqrt{2(1 - \sin\theta)}. \tag{4}$$

The ACA θ^a measurement in such a system may be performed by fixing the vertical position of the three-phase CL with respect to the liquid level far from the plate, after having moved the plate downwards into the liquid pool. Similarly, the RCA θ^r may be obtained from the determination of the three-phase CL after the upward motion. In the case of a random distribution of defects, the CL h is a random function of the plate's position. Therefore, the ACA and the RCA are determined from the averaged CL height $\langle\langle h_i(y)\rangle_y\rangle_i$ by averaging $\langle h(y)\rangle_y$ over multiple equilibrium CLs $\equiv (y, z_i = h_i(y))$, $i = 1, \dots, M$, obtained during consecutive small movements of the plate, in the present results—with $M = 100$ movements each at a step of 2.5 μm corresponding to its immersion in and withdrawal from the liquid container. The procedure for obtaining these angles is detailed and utilized by our team in Ref. [35] for obtaining the CAH on random self-affine rough surfaces.

D. Metastable equilibrium states

According to capillary theory, the metastable meniscus states are determined through minimization of the free energy U of the system, taking into account the capillary and gravitation forces acting in the system. The existence of intrinsic CAH means that roughness (and/or heterogeneity) at two or more length scales (smaller than defects scale) is involved when defining the properties of the solid surface and, respectively, the free energy U of the system. Taking into account the combined effect of the different roughness and/or heterogeneity scales on U is very difficult task, due to the complicated character of the forces, acting at different distances from the CL [36,37]. Young's equation is valid at distances far from the CL, while the effect of van der Walls forces, a charged solid surface, the effect of finite deformability of the solid etc. [2] play role in determining a CA at short distance from the CL, which is different from the CA determined by Young's equation. Even when staying within the phenomenological description of system equilibrium, when taking into account the forces at small distances from the CL, the free energy of the three-phase liquid-gas-solid system from the classical capillary theory needs to be modified (for example, by including the CL tension energy [38]). Along with this, a detailed information on the nature of the roughness and the heterogeneities on scales smaller than the characteristic size of the pillars or holes is needed. In the present work, we adhere to a modification of the capillary theory model to take into account the effect of the intrinsic CAH. According to the capillary model, when the three-phase CL is advancing or withdrawing on a solid surface that is smooth and homogeneous, the macroscopic CA is given by Young's equation. When the solid surface has intrinsic hysteresis, the observable CA is θ_s^a when the CL advances and θ_s^r when the CL recedes on the solid surface. This behavior is similar to having a CL advancing or receding on a smooth and homogeneous solid surface, however, the "Young" CA is considered equal to θ_s^a for advancing CL and to θ_s^r for receding CL, respectively. This simple model allows, in a first approximation, to investigate the influence of the pillars or holes on the CAH, however, it also eliminates some of the important effects that may appear in a more detailed account of roughness and heterogeneity at smaller lengths associated with the change of the transition energy between the possible metastable states [39].

Given the assumptions made, the metastable equilibrium state of the liquid meniscus is determined by minimizing the functional $F(\Sigma)$, dependent on the shape of the liquid and vapor interface Σ, where F is the normalized energy $F = U/\gamma$, defined as

$$F(\Sigma) = \int_\Sigma d\,\Sigma - \cos\theta_B^r \int_{S_B} d\,S_B - \cos\theta_D^r \int_{S_D} d\,S_D + \frac{1}{l_c^2}\int_V z\,dV \tag{5}$$

for withdrawing plate, and

$$F(\Sigma) = \int_{\Sigma} d\,\Sigma - \cos\theta_B^a \int_{S_B} d\,S_B - \cos\theta_D^a \int_{S_D} d\,S_D + \frac{1}{l_c^2}\int_V z\,dV \qquad (6)$$

for immersing plate.

In Eqs. (5) and (6) V is the liquid volume, S_B and S_D are the parts of the plate surface Ξ that belong to the base material and the defect material, respectively, the superscripts r and a refer to the respective receding and advancing contact angles when investigating the case of a withdrawing or immersing plate (for determination of the global RCA/ACA on the microstructured surfaces).

The local minima of Eqs. (5) and (6) are determined numerically using the same step-wise minimization algorithm from our previous studies on the structure of the contact line of the liquid meniscus in contact with a surface featuring periodic [20,21] as well as random [40] defects. In the latter publication, a sequence of equilibrium CLs in the withdrawing mode of the plate was obtained with randomly distributed defects without distance limitations between them (surface with defect distribution type III). We apply the same numerical algorithm here in the current study. We obtain a surface $\Sigma = (x, y, z(x, y)),\ x \geqslant 0$, which minimizes the energy functional (5) or (6), and which is enclosed between the vertical planes $y = 0$ and $y = a$ for two types of boundary conditions (BCs) for the contact of the interface Σ with the enclosing planes $y = 0$ and $y = a$:

— Periodic BCs: $z(x, 0) = z(x, a)$ for every $x \geqslant 0$, and

— Orthogonal BCs: $\partial z(x, y)/\partial y|_{y=0} = \partial z(x, y)/\partial y|_{y=a} = 0$ for every $x \geqslant 0$.

When studying the system with periodic BCs the choice of the defects is made in such a way so that $\theta(0, z) = \theta(a, z)$ for every z. Far away from the heterogeneous plate Ξ (i.e., $x \to \infty$) we impose on the surface $\Sigma = (x, y, z(x, y))$ the condition $z(\infty, y) = 0$.

The periodic surfaces with distribution type IV are investigated using the same algorithm [20] as the one for the surfaces with random defects, but the plate Ξ is periodic with a side length consisting of 30 rows of defects. The initial equilibrium contact line is positioned on two consecutive horizontal rows of defects (15 consecutive defects each). Following the methodology described in Ref. [22], The RCA for pillar-type surfaces and the ACA for hole-type surfaces are determined from the system state where the contact line loses stability, and the entire contact line transitions to a single horizontal row of defects.

III. RESULTS AND DISCUSSION

A. $\theta_B^a = 150^\circ$ for pillar-type surfaces and $\theta_D^a = 150^\circ$ for hole-type surfaces

First, we start with the case when one of the materials is characterized by its unique equilibrium CA of 150°, which is bigger than the ACA on the other material, i.e., $\theta_B^r = \theta_B^a = 150^\circ$ for pillar-type surfaces; $\theta_D^r = \theta_D^a = 150^\circ$ for hole-type surfaces. Note, that the effect on the CAH when $\theta_B^r = \theta_B^a = 150^\circ$ is similar to that when the above angles are 180°, i.e., the angle of the regions between the liquid and the air gaps. The choice of the 150° value for the CA of one of the materials was made for numerical reasons. This is because a CA of 180° between the free surface and the plate creates difficulties in the precise modeling of the virtual displacements of the free surface (note that there are also considerable challenges for the case of CAs close to 180° in experimental studies as well [9,11]). The second material describes a solid surface with which the liquid is in contact. This surface has intrinsic hysteresis, however, with the aim to analyze how the same value of the differences $|\theta_B^a - \theta_D^a|$ and $|\theta_B^r - \theta_D^r|$ affects the ACA and the RCA, correspondingly, we will assume that the CA in Eqs. (5) and (6) for the other material is equal to 100° for all cases. This angle, depending on the direction of the plate displacement (immersing or withdrawing) is interpreted as ACA or RCA, the angles defining the limits of its internal hysteresis interval. Under the above conventions, the Cassie angle θ^C for advancing and receding CL [15] is

$$\theta^C = \arccos(p\cos 100^\circ + (1-p)\cos 150^\circ) \qquad (7)$$

on pillar-type surfaces,

$$\theta^C = \arccos(p\cos 150^\circ + (1-p)\cos 100^\circ) \qquad (8)$$

on hole-type surfaces.

We obtained numerically the ACA and the RCA at defect concentrations ranging from $p = 0.05$ to $p = 0.45$ for circular defects, and $p = 0.34$ for square defects on surfaces with randomly placed defects of distributions types I–III. Also the ACA $\theta^{a(h)}$ (for hole-type surface) and the RCA $\theta^{r(p)}$ (for pillar-type surface) are obtained for periodically distributed defects (distribution type IV). This allows us to obtain the typical features of CAH on surfaces with randomly distributed defects and to compare it to the CAH on surfaces with periodically distributed defects.

1. Independence of the RCA/ACA of the defect shape and defect distribution

Our numerical analysis shows that for all three investigated placements of random defects (distributions type I–III), and for both types of defect shapes—circular and square, the results for the magnitudes of the RCA and ACA are practically the same. This statement is valid for all studied defect concentrations and for both types of heterogeneous surfaces—pillar-type and hole-type. An example in support of this statement is given in Fig. 2, showing the RCA on a pillar-type heterogeneous plate at concentration $p = 0.1$. It shows the dependence of the macroscopic contact angles θ [according to Eq. (3)], for a withdrawing from the liquid pool plate, as functions of the plate displacement number i during 100 plate displacements, each at a step of 2.5 μm (recall that averaging over the magnitudes of θ for many displacements i determines the $\theta^{r(p)}$). In Fig. 2 the results for three types of distributions of circular (shown by bold lines) and square (shown by thin lines) shaped defects are displayed: Type I [solid (black) lines], Type II [dashed (red) lines], and Type III [dotted (blue) lines]. The places where the lines $\theta(i)$ abruptly change their height correspond to instances when the CL has lost stability and transitions to a new location on the plate as a result of a cascade of CL kink depinnings (CL slip mode).

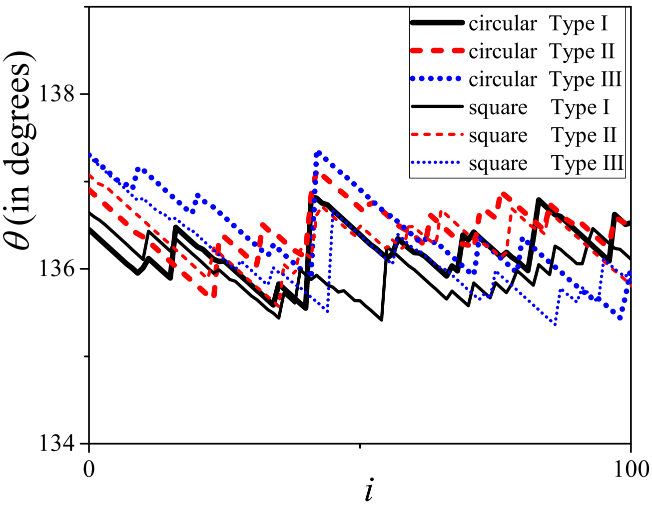

FIG. 2. Macroscopic receding contact angles θ [Eq. (3)] as functions of the displacement number i of the plate discretized upward motion (i.e., receding CLs) for different types of distributions (I–III) and defect shapes (circular and square) on pillar-type surfaces at $p = 0.1$.

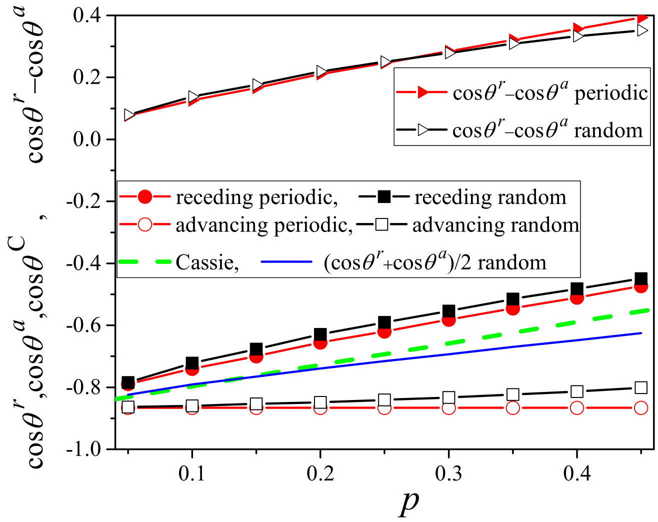

FIG. 3. $\cos\theta^r$ (solid symbols-solid lines) and $\cos\theta^a$ (empty symbols-solid lines) as functions of defect surface concentration p on pillar-type surfaces with randomly distributed (solid and empty squares) and periodically distributed (solid and empty circles) defects. The dashed line is the cosine of Cassie's angle θ^C.

In the rest of the places, the $\theta(i)$ lines have a constant slope, which is related to the CL sticking to the plate surface (CL stick mode) when moving the plate. In the case of a withdrawing hydrophilic plate, the sequence of the equilibrium CLs in the stick-slip regime is shown in a previous publication by our team—see Figs. 2 and 5 in Ref. [40].

We point out that distribution type III actually presents not only circular or square defects, but also defects of complex shape [see Fig. 7(c), where a realization of distribution type III is presented for circular shaped defects]. From the fact that RCA and ACA are the same for the three types of random defect distributions and for both shapes (circular and square) of the defects, it can be concluded that these angles at a given concentration do not depend on the shape of the defects. When investigating how $\theta^{r(p)}$ and $\theta^{a(h)}$ depend on defect concentration, it is more appropriate to study them as functions of defect surface concentration p rather than defect linear concentration ϕ. This is determined by the fact that for placements of circular and square defects having the same total area, i.e., the same defect surface fraction, their linear density will be different. However, in terms of the defect linear density, $\theta^{r(p)}$ and $\theta^{a(h)}$ will have different functional dependencies (while in terms of the defect surface concentration, the dependencies coincide).

2. RCA and ACA as functions of p

In Figs. 3 and 4 we show the obtained results for the cosines of the ACA θ^a [empty squares-(black) solid line], and the RCA θ^r [solid squares-(black) solid line] on pillar-type and hole-type plates, having circular defects placed with distribution type I (i.e., with the maximum distance between the defects), as a function of the defect surface concentration p. The horizontal and vertical axes of both figures have the same scales (for easier comparison of the results). The open (red) circles-solid (red) line and the (red) solid circles-solid (red) line functions show the results for the RCA and the ACA, respectively, for the case where the defects are located on a square grid of horizontal and vertical lines (periodic distribution) (distribution type IV). For this distribution the results for the RCA in Fig. 3 and the ACA in Fig. 4 were obtained numerically by the procedure described above, identifying the moment of kink depinning, and the ACA in Fig. 3 and the RCA in Fig. 4 are represented by the theoretical results, which show that they are equal to 150° and 100°, respectively. The bold dashed (green) lines in Figs. 3 and 4 display the results of the cosine of the Cassie angle θ^C, the thin (blue) line is the half sum of the cosines of the ACA and the RCA in the case of randomly distributed defects.

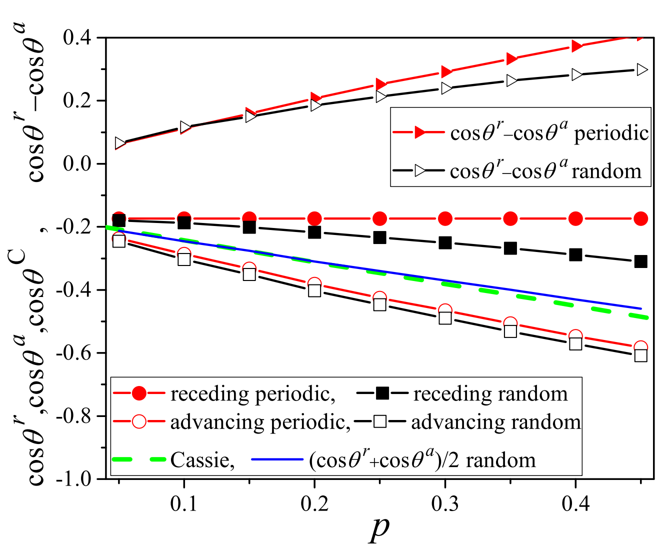

FIG. 4. Same as described in the caption of Fig. 3, except for hole-type surfaces.

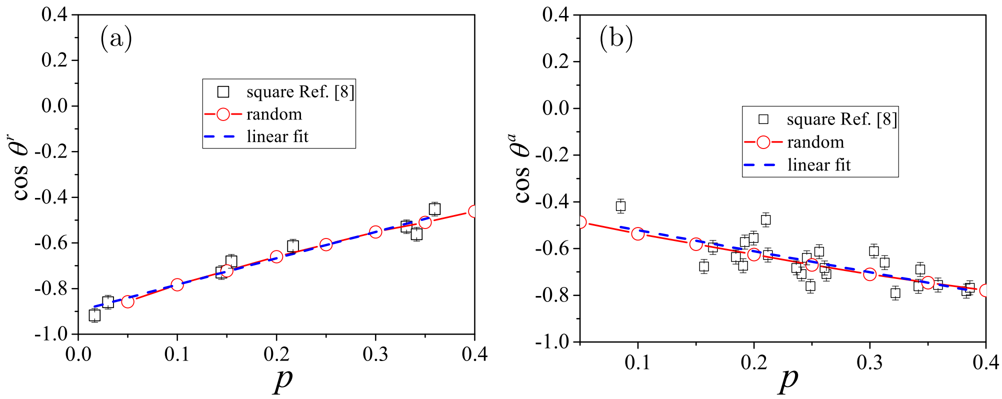

FIG. 5. Cosines of the (a) receding CAs for pillar-type surfaces and (b) advancing CAs for hole-type surfaces as functions of defect surface concentration p on periodic [empty (black) squares] and random [empty (red) circles].

We determine which distribution of defects, random or periodic, has better hydrophobic properties by comparing the magnitudes of the respective differences of the cosines of the CAs: $\cos\theta^r - \cos\theta^a$. This choice is dictated by the fact that not the CAH itself, but the difference $\cos\theta^r - \cos\theta^a$ is proportional to the retention force along the CL and to the critical surface inclination at which the drop with fixed volume begins to slide [41,42]. It is typically desirable to have this difference as small as possible. Our simulation results obtained for $\cos\theta^r - \cos\theta^a$ are displayed in Figs. 3 and 4 for random defect distributions [(black) empty triangles-solid black line] and periodic distribution [(red) solid triangles–solid (red) line].

3. *Pillar-type surfaces*

The main focus has traditionally been on the RCA when studying a surface with pillars. From Fig. 3 it can be seen that the RCA on a surface with randomly distributed defects is smaller than that on a surface with periodically distributed ones, and the difference between the cosines of these angles is small and almost constant independent of the defect concentration. For the ACA, the results show that while in the case of periodic defects the angle is constant and independent of concentration, in the case of random defects it decreases with concentration. The comparison of the difference $\cos\theta^r - \cos\theta^a$, for randomly and periodically distributed defects, presented in Fig. 3, shows that for concentrations up to $p = 0.25$ the $\cos\theta^r - \cos\theta^a$ is the same for both types of distributions, and at higher concentrations the random arrangement of defects leads to a slightly smaller $\cos\theta^r - \cos\theta^a$ than that for periodically spaced defects. For both types of defect arrangements, Cassie's angle θ^C differs from the half sum of θ^a and θ^r. For randomly distributed defects the maximal difference between the dashed and the solid lines in Fig. 3, however, expressed in degrees is about 5°, and for the case of periodic defects it is about 11°.

4. *Hole-type surfaces*

One can observe that Fig. 4 exhibits qualitatively the inverse behavior relative to Fig. 3 with respect to the behavior of the dependencies of the cosines of the RCAs and ACAs on concentration p. In essence, the main features of the ACA/RCA in Fig. 3 (pillar-type surface) are similar to those of RCA/ACA in Fig. 4 (hole-type surface). Therefore, in the present case, as can be seen in Fig. 4, even at concentration of $p = 0.15$ the difference of the cosines $\cos\theta^r - \cos\theta^a$ for random defects is smaller than that for periodic ones, and at greater concentrations it is very large. Also, for random defects the Cassie angle θ^C is close to $(\theta^a + \theta^r)/2$ and, as seen in Fig. 4, the same holds true also for the cosines, $\cos\theta^C$ and $(\cos\theta^a + \cos\theta^r)/2$. Up to concentration $p = 0.25$ one has $(\theta^a + \theta^r)/2 \approx \theta^C$ and with increasing the concentration p the difference slowly increases up to 1.2° (i.e., the difference between the dashed and the solid lines in Fig. 4, however, expressed in degrees).

B. Comparison with the experimental results ($\theta_B^a = 180°$ for pillar-type surfaces and $\theta_D^a = 180°$ for hole-type surfaces)

In the experimental studies of the CL, which a liquid meniscus forms with microstructured surfaces with random controlled disorder—stumps, pores, or chemical defects [43–48] the necessary information for the numerical calculation of the ACA or the RCA in Cassie's regime is not given and a precise comparison with their data for the ACA and the RCA is not possible. However, we will demonstrate that numerical simulations for surfaces with randomly distributed pillars or holes yield results close to the obtained RCAs for pillars and ACAs for holes arranged on periodic lattices in the experimental studies.

In Ref. [8] results are obtained for these angles as functions of the concentration p of the pillars and the holes with a square cross-section of size 20 μm, and when the solid surface has intrinsic hysteresis [95° ± 3°, 116° ± 3°]. The experimental results from this study for the RCA for pillars and the ACA for holes as functions of the defect concentration are reproduced (the solid squares, the error bar corresponds to 3° uncertainty in the CA value) in Figs. 5(a) (Fig. 3(a) in Ref. [8]), and 5(b) (Fig. 4(a) in Ref. [8]), respectively. For easier comparison the vertical axes of Figs. 5(a) and 5(b) have the same scales as the ones in Figs. 3 and 4. The dashed (blue) line is a linear fit (using Origin-software) to the experimental results as function of the concentration p. The results obtained from the numerical simulations for a surface with random defects in these figures are shown by empty circles-solid lines, and when

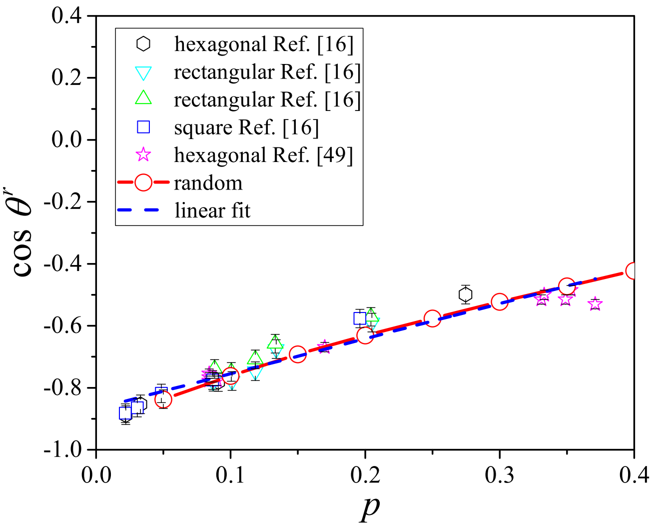

FIG. 6. Cosines of the RCAs as functions of surface concentration p of pillar defects on randomly heterogeneous surface—empty (red) circles, compared to periodically distributed pillars on surfaces with square, rectangular and hexagonal arrangement of pillars.

studying the RCA in the energy functional Eq. (5) the contact angles $\theta_D^r = 95^\circ$, $\theta_B^r = 180^\circ$ are used, and for the study of ACA $\theta_D^a = 180^\circ$, $\theta_B^a = 116^\circ$ in Eq. (6). One can see that there is a close agreement between the numerical results for the CAs for randomly distributed defects and the linear fit for periodic defects (experimental results) for both types of surfaces, i.e., surfaces with pillars and surfaces with holes.

Most experimental studies are limited to studies of surfaces with pillars. In Refs. [22] and [16], as was mentioned in the Introduction, it is demonstrated experimentally, that for different periodic pillar arrangement patterns—square, rectangular and hexagonal lattices (in the case of circular defects, with 10 μm diameter) one arrives at the same dependence of the RCA as function of the surface concentration. These results (with error bars) for surfaces with pillars made of material with intrinsic hysteresis whose RCA is 89°, are shown in Fig. 6 (see Fig. 3 in Ref. [16]) [(blue) squares for square lattice, (cyan) and (green) triangles for rectangular lattices, and (black) hexagons in the case of hexagonal lattices]. Close to a RCA of $91^\circ \pm 2^\circ$ for the intrinsic hysteresis of the pillars material, the surface with the hexagonally arrayed circular (diameter from 20 to 40 μm) micropillars, for which experimentally is obtained the RCA at different pillar (surface) concentrations [49]. These results (from Fig. 5 in Ref. [49]) are presented in Fig. 6 with five-pointed solid (magenta) stars. The vertical axes of Fig. 6 have the same scale as the ones in Figs. 3–5. The dashed (blue) line is a linear fit (using Origin software) to the experimental results as function of the surface concentration p. Since, as we illustrated in Fig. 3, the RCAs on surfaces with randomly spaced pillars and periodically spaced ones, are close, it should be expected that the numerical simulations for the RCA on surfaces with random defects will also be close to the above experimental data. Indeed, the numerical simulations results obtained for $\theta_D^r = 89^\circ$, $\theta_B^r = 180^\circ$ in the case of randomly distributed defects, shown in Fig. 6 by empty (red) circles-solid lines confirms this assumption.

IV. CONCLUSIONS

The advancing and receding equilibrium contact angles are investigated numerically for a liquid in contact with an ultrahydrophobic surface with randomly distributed pillars or pores in the Cassie's wetting regime. The free surface of the liquid meniscus was obtained in the framework of the heterogeneous surface approximation model for a broad interval of values of the pillar or hole concentration for micropillars or holes of both square and circular cross sections. The equilibrium contact lines and the contact angles which the liquid forms with them are investigated for three types of random placing of the defects on the plate—two with restrictions (1) with maximum and (2) with minimum distance between the defects), in these cases the defects are isolated, and (3) without restrictions (the defects can overlap). By simulating the downward and upward motion of the plate, the advancing and receding contact angles for the three types of defect placements were obtained. The results show that the type of

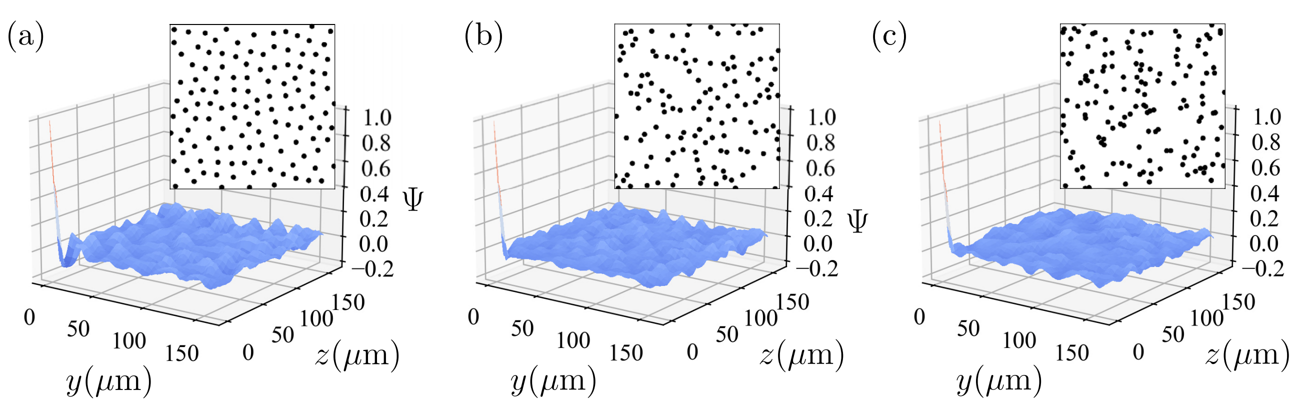

FIG. 7. Short range 2D defect autocorrelation function $\Psi(y, z)$ in a square domain 320 μm × 320 μm for circular defects at concentration $p = 0.1$ is shown for defect distribution: (a) type I, (b) type II, (c) type III (without a distance condition imposed).

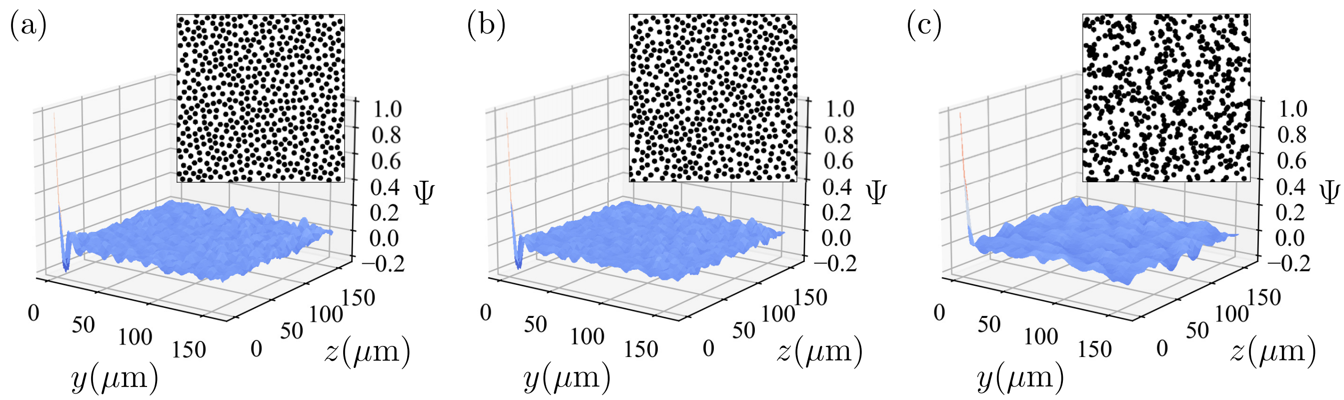

FIG. 8. Same as described in the caption of Fig. 7, except at concentration $p = 0.4$.

defect distribution and also the shape of the defects (circular or square cross-section) does not affect the magnitude of the two angles. The obtained results are compared with the values for ACA and RCA on surfaces with periodically spaced defects, which are experimentally obtained and also through numerical simulations.

The results of the numerical simulations showed that the retention force for a plate with randomly located defects is not greater, and for larger concentrations of defects, it is smaller than that for periodically spaced ones. Thus, a liquid drop on surface with random defects will start rolling at a smaller angle of surface inclination than on a surface with periodic defects. Comparisons with experimental results for the receding contact angle on a surfaces with pillars and with the advancing contact angle on surfaces with periodically arranged holes showed that the corresponding contact angles obtained with a random arrangement of physical defects are close to those with periodically arranged ones. The same conclusion has recently been drawn experimentally for surfaces with pillars, when the wetting is in the Wenzel's wetting regime [45].

New experimental studies for surfaces with randomly located defects are needed to more accurately and comprehensively verify the results of the numerical simulations. This can be done both, by extensions of the research in Refs. [45,46,48], and by direct comparison of the angle at which drops on an inclined plane with periodically spaced and randomly spaced defects lose equilibrium.

APPENDIX: DEFECT CORRELATIONS

The autocorrelation functions of the obtained defect distributions (types I–III) are calculated using the method from Ref. [50]. Typical results for the short-range 2D autocorrelation functions $\Psi(y, z)$ on a square domain $320\,\mu m \times 320\,\mu m$ in coordinate system (y, z) are shown for circular defects in Fig. 7 at concentration $p = 0.1$ and in Fig. 8 at concentration $p = 0.4$. In Figs. 7(a) and 8(a), 7(b) and 8(b), and 7(c) and 8(c), example defect distributions and autocorrelations for distributions type I–III, correspondingly, are shown.

The analyzed realizations of the defect distributions are shown in the inset of each corresponding figure. The results show that the correlation at a distances bigger than the defect diameter $2r$ is small (i.e., it is short range $|\Psi| < 0.2$) for all cases I–III), and moreover, Ψ does not show any sign of periodicity. The presence of a high peak (i.e., $\Psi \approx 1$) when $(y, z) \to (0, 0)$ reflects the correlation of the defect with itself. Therefore, no short-range periodic fluctuations in Ψ can be observed in any direction for all analyzed cases. When the domain size is increased, i.e., for long-range correlations, the amplitude of Ψ decreases.

[1] D. Quéré, Annu. Rev. Mater. Res. **38**, 71 (2008).
[2] P. G. de Gennes, Rev. Mod. Phys. **57**, 827 (1985).
[3] A. Marmur, C. Della Volpe, S. Siboni, A. Amirfazli, and J. Drelich, Surf. Innovations **5**, 3 (2017).
[4] H. Y. Erbil, Surf. Sci. Rep. **69**, 325 (2014).
[5] D. Öner, and T. J. McCarthy, Langmuir **16**, 7777 (2000).
[6] F. Wang, Y. Wu, and B. Nestler, Adv. Mater. **35**, 2210745 (2023).
[7] L. Barbieri, E. Wagner, and P. Hoffmann, Langmuir **23**, 1723 (2007).
[8] C. Priest, T. W. J. Albrecht, R. Sedev, and J. Ralston, Langmuir **25**, 5655 (2009).
[9] N. A. Patankar, Langmuir **26**, 7498 (2010).
[10] N. N. Anantharaju, M. V. Panchagnula, and S. Vedantam, Langmuir **25**, 7410 (2009).
[11] C. Dorrer and J. Rühe, Langmuir **22**, 7652 (2006).
[12] B. R. Prabhala, M. V. Panchagnula, and S. Vedantam, Colloid Polym. Sci. **291**, 279 (2013).
[13] P. Dimitrakopoulos and J. Higdon, J. Fluid Mech. **395**, 181 (1999).
[14] M. J. Santos and J. A. White, Langmuir **27**, 14868 (2011).
[15] C. W. Extrand, Langmuir **19**, 3793 (2003).
[16] M. Rivetti, J. Teisseire, and E. Barthel, Phys. Rev. Lett. **115**, 016101 (2015).
[17] C. Extrand, Langmuir **18**, 7991 (2002).

[18] R. Raj, R. Enright, Y. Zhu, S. Adera, and E. N. Wang, Langmuir **28**, 15777 (2012).
[19] C. Dorrer and J. Rühe, Langmuir **23**, 3179 (2007).
[20] S. Iliev and N. Pesheva, Phys. Rev. E **93**, 062801 (2016).
[21] S. Iliev, N. Pesheva, and V. S. Nikolayev, Phys. Rev. E **90**, 012406 (2014).
[22] A. Gauthier, M. Rivetti, J. Teisseire, and E. Barthel, Phys. Rev. Lett. **110**, 046101 (2013).
[23] K. Brakke, Exp. Math. **1**, 141 (1992).
[24] S. Iliev, N. Pesheva, and P. Iliev, Phys. Rev. E **101**, 052801 (2020).
[25] G. Carbone and L. Mangialardi, Eur. Phys. J. E **16**, 67 (2005).
[26] C. W. Extrand, Langmuir **27**, 6920 (2011).
[27] O. Vinogradova and A. Dubov, Mendeleev Commun. **22**, 229 (2012).
[28] H.-J. Butt, J. Liu, K. Koynov, B. Straub, C. Hinduja, I. Roismann, R. Berger, X. Li, D. Vollmer, W. Steffen, and M. Kappl, Curr. Opin. Colloid Interface Sci. **59**, 101574 (2022).
[29] H. J. Ensikat, Langmuir **28**, 14338 (2012).
[30] K. Grundke, K. Pöschel, A. Synytska, R. Frenzel, A. Drechsler, M. Nitschke, A. L. Cordeiro, P. Uhlmann, and P. B. Welzel, Adv. Colloid Interface Sci. **222**, 350 (2015).
[31] Y. Jiang and C.-H. Choi, Adv. Mater. Interfaces **8**, 2001205 (2020).
[32] A. W. Adamson and A. P. Gast, *Physical Chemistry of Surfaces* (Wiley, New York, NY, 1997).
[33] R. David and A. Neumann, Langmuir **29**, 4551 (2013).
[34] L. D. Landau and E. M. Lifshitz, *Fluid Mechanics* (Pergamon Press, Oxford, UK, 1987).
[35] S. Iliev, N. Pesheva, and P. Iliev, Phys. Rev. E **107**, 024802 (2023).
[36] M. Rauscher and S. Dietrich, Annu. Rev. Mater. Res. **38**, 143 (2008).
[37] D. Bonn, J. Eggers, J. Indekeu, J. Meunier, and E. Rolley, Rev. Mod. Phys. **81**, 739 (2009).
[38] A. Tinti, A. Giacomello, S. Meloni, and C. M. Casciola, J. Chem. Phys. **158**, 134708 (2023).
[39] R. C. Remsing, E. Xi, S. Vembanur, S. Sharma, P. G. Debenedetti, S. Garde, and A. J. Patel, Proc. Natl. Acad. Sci. USA **112**, 8181 (2015).
[40] S. Iliev, N. Pesheva, and P. Iliev, Eur. Phys. J. E **45**, 66 (2022).
[41] G. Macdougall and C. Ockrent, Proc. R. Soc. London Ser. A **180**, 151 (1942).
[42] C. G. L. Furmidge, J. Colloid Sci. **17**, 309 (1962).
[43] A. Prevost, E. Rolley, and C. Guthmann, Phys. Rev. B **65**, 064517 (2002).
[44] E. Rolley, C. Guthmann, R. Gombrowicz, and V. Repain, Phys. Rev. Lett. **80**, 2865 (1998).
[45] P. Kumar, P. Mulvaney, and D. J. E. Harvie, J. Colloid Interface Sci. **659**, 105 (2024).
[46] E. Bormashenko, A. Musin, G. Whyman, Z. Barkay, and M. Zinigrad, Langmuir **29**, 14163 (2013).
[47] E. Bormashenko, A. Musin, G. Whyman, Z. Barkay, and M. Zinigrad, Eur. Phys. J. E **38**, 2 (2015).
[48] S. Moulinet, C. Guthmann, and E. Rolley, Eur. Phys. J. E **8**, 437 (2002).
[49] B. M. L. Koch, A. Amirfazli, and J. A. W. Elliott, J. Phys. Chem. C **118**, 18554 (2014).
[50] E. Bormashenko, A. Malkin, A. Musin, Ye. Bormashenko, G. Whyman, N. Litvak, Z. Barkay, and V. Machavariani, Macromol. Chem. Phys. **209**, 567 (2008).